Available online at www.sciencedirect.com
ScienceDirect
Energy Reports 8 (2022) 135–145
www.elsevier.com/locate/egyr

2022 International Conference on the Energy Internet and Energy Interactive Technology (EIEIT 2022), March 25–27, 2022, Wuhan, China

Research on wave energy collection based on swing ship triboelectric nanogenerator

Yinghao Zhong[a], Jin Yan[a,b,*], Naerduo Mei[a], Chao Huang[a]

[a] *Guangdong Ocean University, Zhanjiang, Guangdong, 524088, China*
[b] *Shenzhen Research Institute of Guangdong Ocean University, Shenzhen, Guangdong, 518120, China*

Received 22 September 2022; accepted 5 October 2022
Available online 22 October 2022

Abstract

Wave energy has the advantages of huge energy storage and high energy flow density, and it is one of the most promising Marine renewable resources. In this paper, a design method based on swing ship type triboelectric nanogenerator (ST-TENG) is proposed to collect low-frequency wave energy. This swing ship type TENG (ST-TENG) contains three sets of triboelectric nanogenerator, consisting of internal and external ship type devices with pasted electrodes and independent rollers. Combined with the power generation theory of two working modes of free-standing layer and vertical contact separation and COMSOL electrostatic simulation, the operating principle of the device is clarified. Through the rolling of the roller in the built-in ship and the swing of the built-in ship, the wave energy can be effectively collected and transformed into electric energy. In addition, through the comparative experiment, the influence of different influencing factors on the output performance of ST-TENG is quantitatively analyzed. The experimental results show that for the internal structure parameters, ST-TENG has the best output capacity in the case of polytetrafluoroethylene (PTFE) with thickness of 0.3 mm, solid cylinder and adding foam tape. Under external working conditions, 1.5 Hz is closest to the resonant frequency of the ST-TENG, and the amplitude increases from 30 mm to 60 mm, which improve the power generation performance. In addition, ST-TENG can illuminate at least 100 LEDs under normal conditions and quickly charge different capacitors to a certain voltage. Therefore, the design of ST-TENG provides new ideas for large-scale blue energy collection.

Peer-review under responsibility of the scientific committee of the International Conference on the Energy Internet and Energy Interactive Technology, EIEIT, 2022.

Keywords: Wave energy; Triboelectric nanogenerator; COMSOL; Blue energy

1. Introduction

In order to solve a series of problems such as environmental pollution, global warming and energy depletion caused by traditional fossil energy, developing green energy sources, and expanding the supply of new energy sources have become the common goals of the world [1]. Wave energy has become the focus of the research and

* Corresponding author at: Guangdong Ocean University, Zhanjiang, Guangdong, 524088, China.
E-mail address: yanj@gdou.edu.cn (J. Yan).

https://doi.org/10.1016/j.egyr.2022.10.073

Peer-review under responsibility of the scientific committee of the International Conference on the Energy Internet and Energy Interactive Technology, EIEIT, 2022.

development of marine renewable resources because of its rich reserves, high energy density, low environmental impact, high grade, and wide distribution [2]. Conventional wave power generation technology often converts wave motion into rotating or linear motion by means of switching structures to drive electromagnetic generators for power generation [3], However, these power generation methods have disadvantages such as high maintenance cost, low conversion efficiency and cumbersome structure [4–6], Therefore, adopting the new wave energy collection method has become an important research direction.

Triboelectric Nanogenerator (TENG) was proposed by Professor Wang of Georgia Institute of Technology in 2012 that mechanical energy can be efficiently converted into electrical energy by combining friction electrification effect with electrostatic induction and output in the form of electrical signals [7–17]. Using the operating principle of TENG and the design of different structures, scholars at home and abroad have conducted comprehensive research in the domain of wave energy collection [18–23]. Wang et al. [24] designed a freestanding fully closed rolling triboelectric nanogenerator, which was able to drive more than 70 light-emitting diodes directly at a duty cycle of 26.5% due to the outstanding charge transfer efficiency of freestanding structure and less friction rolling structure and commercial thermometers. By optimizing the material and structural design, Cheng et al. [25] improved the traditional hard contact spherical triboelectric nanogenerator into a soft contact type, thus increasing the maximum output charge by tenfold due to the increased contact area. Xu et al. [26]proposed a high-power density TENG, which adopts a tower structure to obtaining low-frequency wave energy in any direction. The TENG unit of the device can be considered as a current source with high relative load impedance, and the power density augment proportionally to the augment of parallel units that are not connected to the rectifier. A planar triboelectric nanogenerator network consisting of spring-loaded tape and triple layered polymer film was designed by Liu et al. [27] to effectively avoid seawater erosion of transmission lines and tangling between TENG units when collecting wave energy on a large scale. These studies provide a good reference for wave energy collection techniques.

2. Structure and principle

2.1. ST-TENG basic structure

Combining the operating principle of contact separation and free-standing layer mode TENG, a swing ship type Triboelectric Nanogenerator (ST-TENG) is proposed in this paper. Fig. 1(a) show that the integral structure of ST-TENG consists of an internal ship type unit, an external ship type device and separate roller, which includes three groups of triboelectric nanogenerator (Fig. 1(b)). The first group of triboelectric nanogenerator is a freestanding structure (F-TENG) including nylon roller with electrodes on the surface, polytetrafluoroethylene (PTFE), aluminum electrodes, foam tape as well as an internal ship type apparatus made from polylactic acid (PLA) materials. By rolling the aluminum electrode surface affixed to the inner surface of the built-in ship type device by the nylon roller acting as an independent moving layer, the potential between the two electrodes on the inner surface of the built-in ship type device changes periodically, thus generating an inductive current on the external load connecting the two electrodes. The second and third groups of triboelectric nanogenerator use contact separation structure (CS-TENG), which includes electrodes pasted on the outer surface of the built-in ship type apparatus, Teflon,

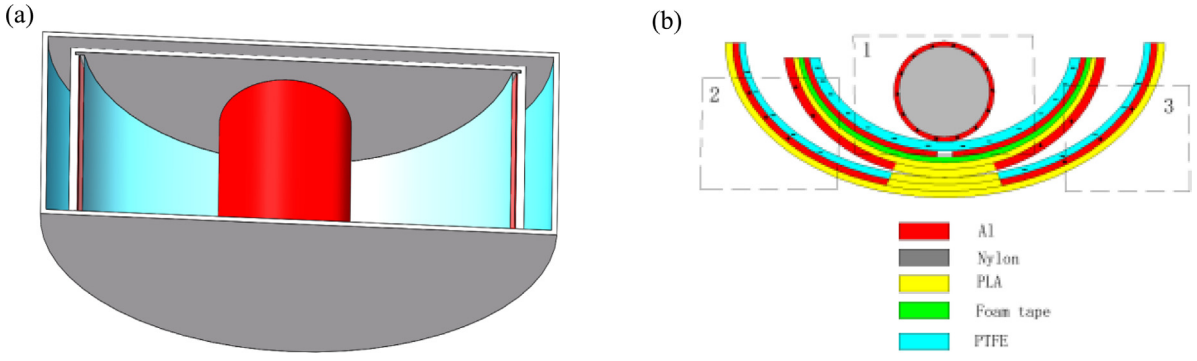

Fig. 1. (a) Integral structure diagram of ST-TENG; (b) The schematic diagram of ST-TENG internal structure.

and electrodes pasted on the inner surface of the external ship type apparatus. The principle is that through the left–right swing of the built-in ship type device, the electrode on the outer surface of the device is contacted and separated from the PTFE plated with another electrode on the back, so that the electric potential disparity between the two electrodes is generated, and then the induced current is generated. ST-TENG can effectively collect low-frequency, irregular wave energy through the rolling of a wave driven roller as well as the swinging of a ship type device.

2.2. ST-TENG basic structure

Fig. 2 shows the power generation principle of F-TENG. By adding external excitation (such as ocean waves), the roller scrolls back and forth on the inner surface of the built-in ship type device. After multiple cycles of friction with PTFE, since PTFE and aluminum are in different electrode sequence, Al and PTFE films have positive and negative charges respectively, and since the PTFE film is electret, the charge can be retained on its surface for a long time. As shown in Fig. 2 (a–b), when the roller serving as an independent electrode roll from the left to the middle, negative charge is sensed on the left electrode, resulting in potential difference on the left and right sides. In order to balance the electric potential disparity, the external circuit will transfer electrons to generate current, and as the roller rolls to the right, the current flows from the right electrode to the left electrode. On the contrary, when the roller rolls from right to left (Fig. 2 (C–D)), The electrons are refluxed and the current flows from the left electrode to the right electrode. The roller can reciprocate and roll between the left and right electrodes by excitation to generate alternating current in the external circuit.

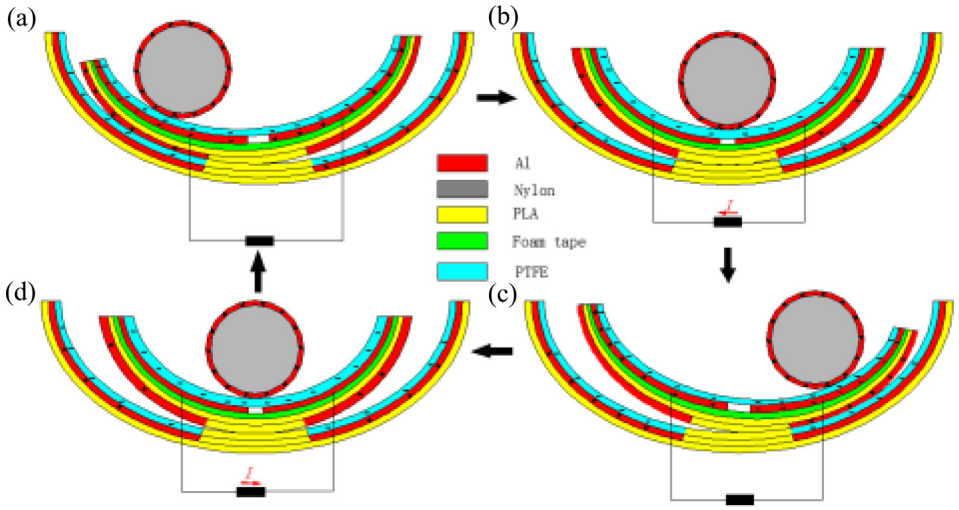

Fig. 2. Operating principle of the F-TENG.

The operating principle of the second and third sets of triboelectric nanogenerator (CS-TENGs) is the same. The second set of examples is used here. As shown in Fig. 3, the external excitation (such as ocean waves) causes the roller to scroll back and forth on the inner surface of the built-in ship type device and causes the built-in ship type device to swing left and right as the roller rolls. Similarly, when the outer surface electrodes of the device rub against the PTFE film for several cycles, PTFE and Al electrodes are negatively and positively charged respectively. When the built-in ship type device swings from left to right (Fig. 3 (a–b)), PTFE is separated from the aluminum electrode to balance the electric potential disparity between the two electrodes. Current is generated in the external circuit and flows from the built-in ship type outer surface electrode to the outer ship type inner surface electrode. When the built-in ship type device swings from right to left, the opposite current is generated (Fig. 3 (c–d)). The built-in ship type device can swing left and right by excitation to produced alternating current in the out-of-electrode circuit.

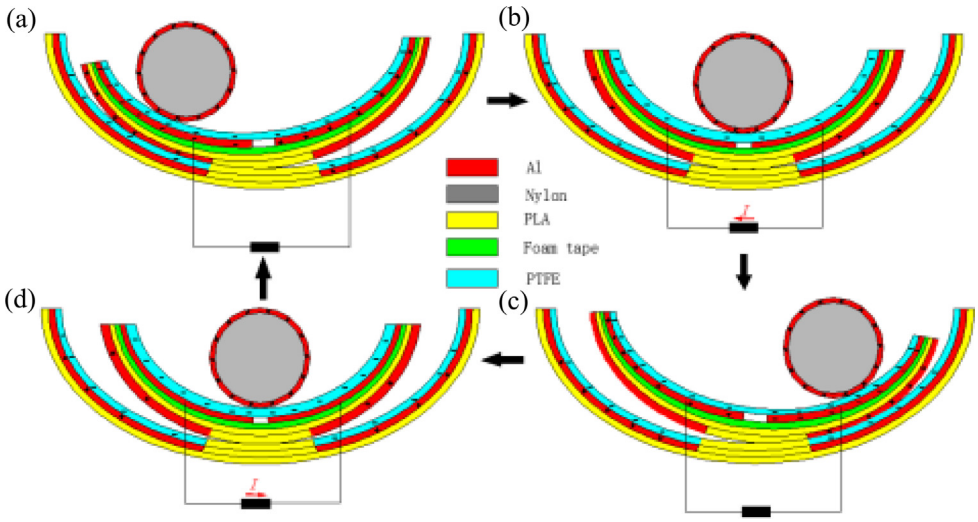

Fig. 3. Operating principle of the CS-TENG.

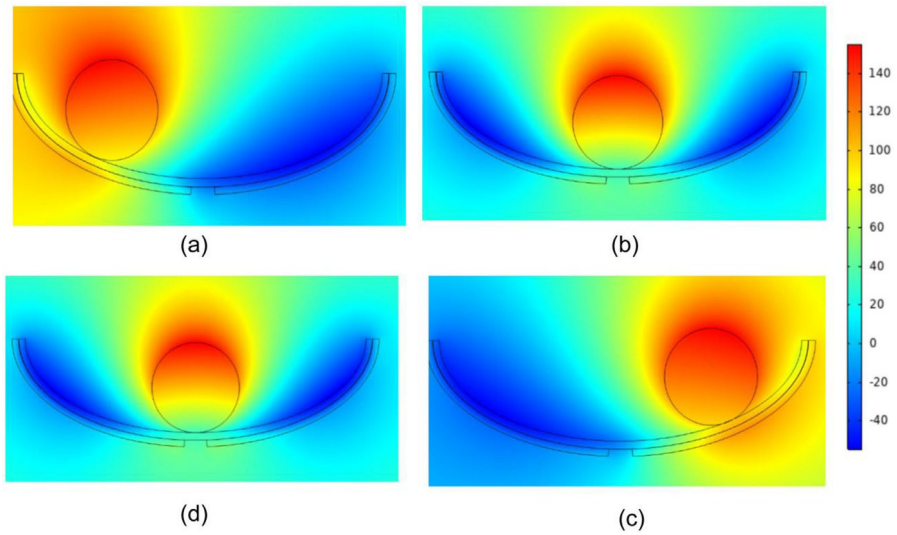

Fig. 4. Schematic diagram of simulated potential distribution.

2.3. Electrical performance simulation based on COMSOL Multiphysics

Using COMSOL Multiphysics software, the potential distribution of the roller at two induction electrodes in different motion positions can be calculated by Maxwell's control equation. As shown in Fig. 4, the electric potential disparity between the two induction electrodes can be clearly displayed. Due to the existence of electric potential disparity, electrons are transferred at the positive and negative electrodes through the external circuit, resulting in current.

3. Experimental results and discussion

An experimental study on the generation characteristics of ST-TENG is conducted by using a linear motor to simulate the wave driving ST-TENG. Fig. 5 shows the composition diagram of the experimental system based on linear motor, by setting different acceleration and displacement and thereby controlling driving parameters such as

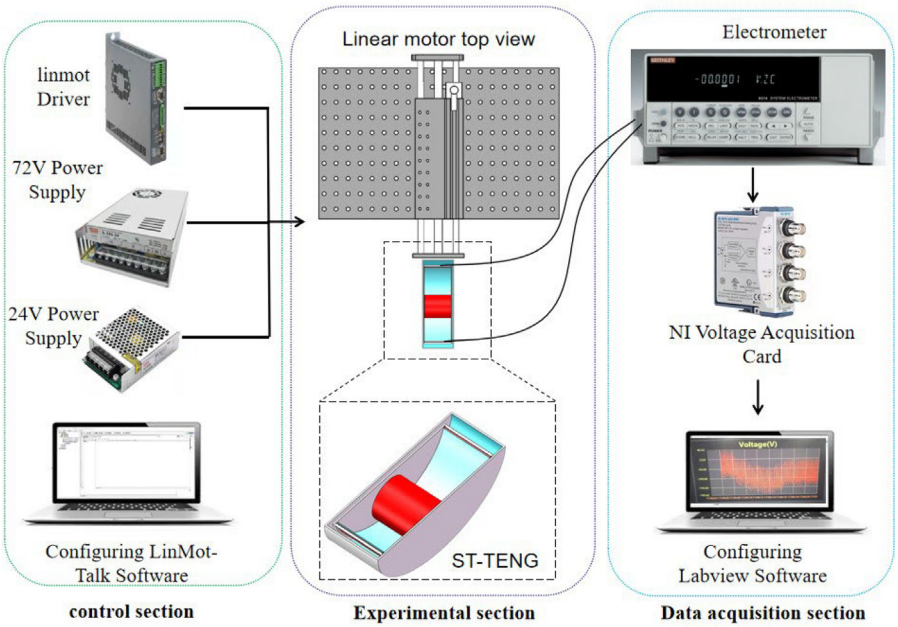

Fig. 5. Schematic diagram of experimental system.

frequency and amplitude, the ST-TENG was fixed to a linear motor driver rod to drive the ST-TENG movement. The effects of different factors on ST-TENG power generation capacity were studied.

3.1. The influence of the dielectric materials on F-TENG output capacity

By controlling the parameters of linear motor to ensure the consistency of external working conditions, the frequency is set as 2 Hz and the amplitude is 40 mm. Here, 0.08 mm FEP film and PTFE film as well as 0.3 mm PTFE film are selected. As can be seen from Fig. 6(a), when the thickness is 0.08 mm, the open circuit voltage of PTFE is slightly higher than FEP because the open circuit voltage depends on the distance between the roller and the dielectric material and the distance between the two induction electrodes, and the material itself has little effect on it. Fig. 6(b) and (c) show that the peak short-circuit current of PTFE is 47% higher than that of FEP, and the short-circuit transfer charge is nearly 30%. This is because PTFE and FEP have different triboelectric sequence positions and electronegativity, PTFE is easier to lose electrons than FEP. Therefore, the stronger the

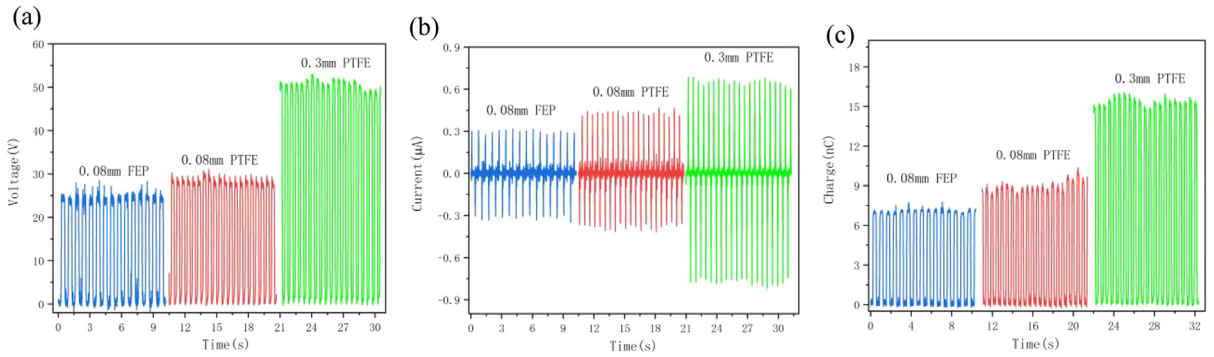

Fig. 6. The variation of F-TENG output signal under different dielectric films (a) Open circuit voltage V_{OC};(b) short circuit current I_{ST}; (c) transferred charge quantity Q.

transfer charge ability, the higher the output performance. In addition, when the thickness of PTFE increases from 0.08 mm to 0.3 mm, the output electrical signal increases. This is because after the film thickens, it can capture more friction charges and produce higher output.

3.2. Effect of roller weight on the output performance of F-TENG

After studying the influence of dielectric film on the power generation performance of F-TENG, the influence of roller weight on the power generation performance of F-TENG is further studied. Select solid and hollow roller for the experiment. At the same time, 0.3 mm PTFE film is selected with control frequency of 2 Hz and amplitude of 40 mm. The output performance of solid roller shown in Fig. 7 is much larger than that of hollow roller, among them, the peak open circuit voltage and peak short-circuit current of the solid roller are more than 2 times higher, and the peak transfer charge is more than 3 times higher. This is because the weight of the solid roller is large, so that the Al roller can fully rub and contact with the PTFE film, and the inertia increases the movement speed of the roller and the charge transfer efficiency, thus the current output increases.

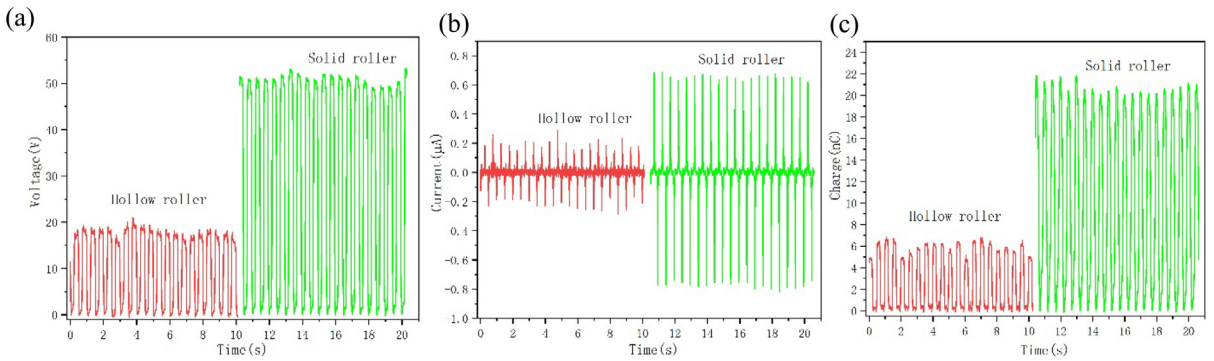

Fig. 7. The variation of F-TENG output signal under different weight rollers (a) Open circuit voltage V_{OC}; (b) short circuit current I_{ST}; (c) transferred charge quantity Q.

3.3. Effect of foam tape addition on the output performance of F-TENG

After studying the influence of dielectric material and roller weight on the output performance of F-TENG, in order to further increase the F-TENG output performance, we can add a layer of foam tape at the bottom of the two induction electrodes. The other experimental conditions were unchanged, here the solid drum was chosen, and the dielectric material was chosen to make 3 mm PTFE film, the same control frequency was 2 Hz, the amplitude was 40 mm, and the results were shown in Fig. 8, The F-TENG peak open voltage increased from 53.09 V to 90.40

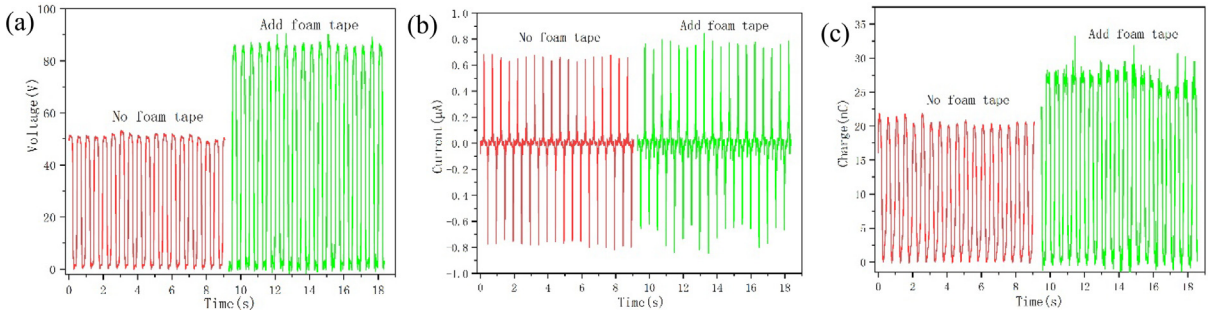

Fig. 8. The variation of F-TENG output signal after adding foam tape (a) Open circuit voltage V_{OC}; (b) short circuit current I_{ST}; (c) transferred charge quantity Q.

V (Fig. 8(a)), the peak short-circuit current was essentially unchanged (Fig. 8(b)), and the peak transferred charge increased from 21.89 NC to 33.17 NC (Fig. 8(c)). This is because the short-circuit current depends on the amount of charge transfer in unit time, while the addition of foam tape because of its elasticity can increase the friction area and charge areal density between roller and dielectric material, but it does not affect the charge transfer efficiency, thus will make the output voltage, and transferred charge increase and will have little effect on the short-circuit current.

3.4. Effect of foam tape addition on the output performance of F-TENG

The weight of the roller not only affects the output performance of F-TENG, but also has a certain impact on the output performance of CS-TENG. In order to study the specific impact, under the condition of ensuring the consistency of other conditions, the electrode width is 7.3 cm, the length is 7.5 cm, the dielectric material is still PTFE film, and the parameter setting frequency of linear motor is controlled to be 1.5 Hz, and the amplitude is 60 mm, the results of testing the output performance of hollow and solid rollers on CS-TENG are shown in Fig. 9. When using hollow rollers, the peak open circuit voltage of CS-TENG is 55.85 V, which is 18% lower than the 65.81 V peak open circuit voltage output of solid rollers (Fig. 9(a)). In addition, from Fig. 9(c), when using solid rollers, the peak transfer charge of CS-TENG increases from 23.18 nc to 34.40nc, which is nearly 50%, This is because the use of solid roller will make the contact friction of CS-TENG closer and improve the surface density of charge, which can greatly improve the amount of charge transfer and voltage. It can be seen from Fig. 9(b) that the current changes little, because the size of CS-TENG current is determined by the swing frequency of the built-in ship type device, and the roller weight has little effect on the swing frequency.

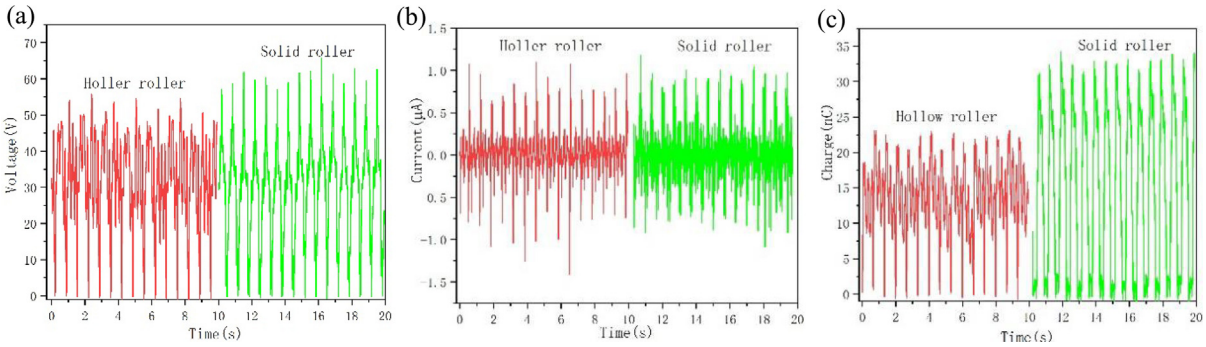

Fig. 9. The variation of CS-TENG output signal under different weight rollers (a) Open circuit voltage V_{OC}; (b) short circuit current I_{ST}; (c) transferred charge quantity Q.

3.5. The influence of the frequency on ST-TENG output capacity

After studying the influence of internal structural conditions on the output performance of ST-TENG, the influence of external conditions on the output performance of ST-TENG is further studied. First, the effect of frequency on the output performance of ST-TENG is studied. Under the condition of ensuring the same internal structural conditions, the solid cylinder is selected, 0.3 mm PTFE is used as dielectric film, and foam tape is added to increase the contact area. When the fixed amplitude is 60 mm, explore the output performance of ST-TENG in the frequency range of 1–2.5 Hz.

It is found in the experiment that the open circuit voltage of F-TENG is the largest when the frequency is 1.5 Hz, and the peak value can reach 107 V (Fig. 10(a)), and then it decreases at 2 Hz and 2.5 Hz. From the specific experimental phenomenon, it can be clearly found that when the frequency is 1.5 Hz, the rolling area of the roller is the largest, so the charge area density increases and the voltage also increases, and it is inferred that 1.5 Hz is close to the resonance frequency of the device. Similarly, when the frequency is close to the resonance frequency, the amount of transferred charge and short-circuit current also increase at the same time (Fig. 10(b) and (c)). Currently, the peak amount of transferred charge and peak short-circuit current are 35.91 nc and 1.74 μA

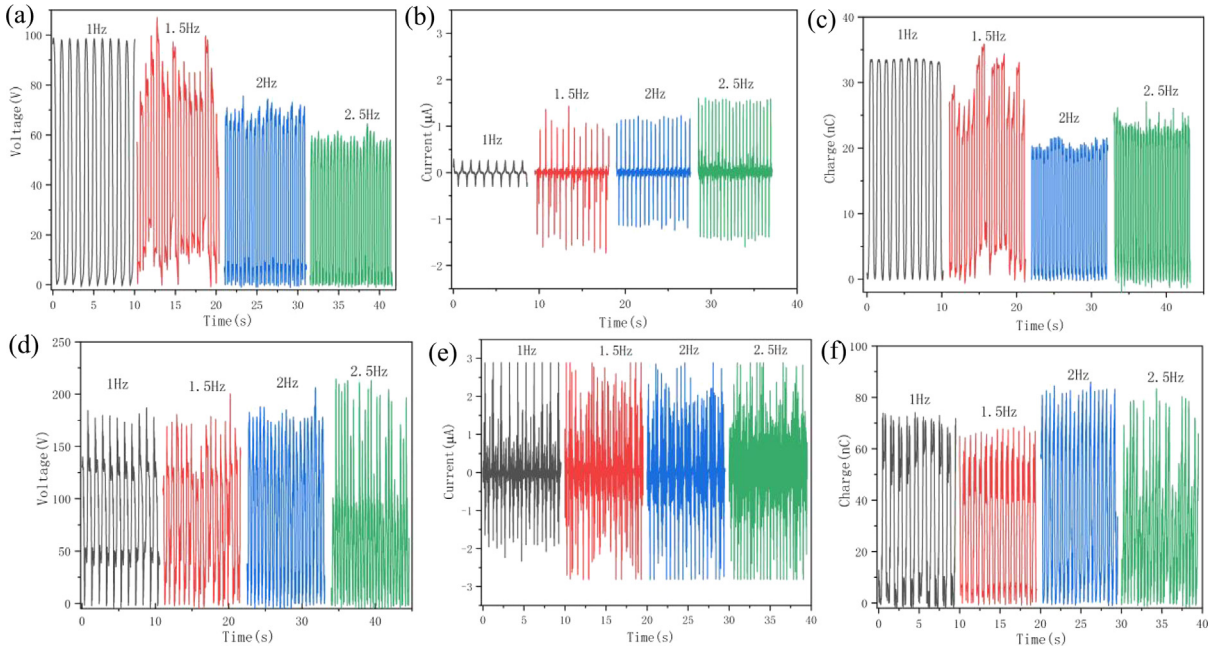

Fig. 10. The variation of ST-TENG output signal under different frequency working conditions (a) F-TENG Open circuit voltage V_{OC}; (b) F-TENG short circuit current I_{ST}; (c) F-TENG transferred charge quantity Q; (d) CS-TENG Open circuit voltage V_{OC}; (e) CS-TENG short circuit current I_{ST}; (f) CS-TENG transferred charge quantity Q.

respectively. This is because the charge transfer speed between Al roller and PTFE film increases near the resonance frequency, resulting in the increase of induced short-circuit current. As can be seen from Fig. 10(d) and (f), in the case of 2 Hz, the voltage and charge signals are not only relatively stable, but also have high output. This is because the external frequency increases, the speed of the roller increases, and the swing range of the swing ship type device will also increase, resulting in the increase of the contact area between the electrode and PTFE. As can be seen from Fig. 10(e), the short-circuit current of CS-TENG changes little with the change of frequency.

3.6. Effect of amplitude on output performance of ST-TENG

Firstly, the internal structure condition is consistent. Solid roller, dielectric film 0.3 mm PTFE and foam tape are used to increase output. Because 1.5 Hz is close to resonance frequency, the output signal is not stable at this frequency. 1 Hz is used to investigate ST-TENG output performance at 30-60 mm amplitude range. Fig. 11(a) and (c) show that the output voltage and output charge of F-TRNG gradually enhance with increasing amplitude due to the increased amplitude which increases the area over which the roller rolls, thus increasing the F-TENG voltage and transfer charge. As shown in Fig. 11(b), the induced short-circuit current increases slightly with increasing amplitude, which is due to the larger amplitude, the greater inertial acceleration of the roller, thus accelerating charge transfer and thus increasing short-circuit current. As shown in Fig. 11(d) and (f), the open-circuit voltage and transfer charge also increase as the amplitude increases from 30 mm to 60 mm, due to the increased amplitude which increases the swing amplitude of the built-in swing ship, thereby increasing the contact area between the CS-TENG electrode and the PTFE. Short-circuit current increases first and then remains unchanged (Fig. 11(d)) as the amplitude increases and the roller acceleration increases, thus increasing the swing frequency of the built-in type swing device and maximizing it at 50 mm.

3.7. Experiments of capacitive charging and lighting

In order to verify the actual power generation capacity of ST-TENG, this paper conducts experimental verification and analysis at the frequency of 1 Hz and the amplitude of 60 mm. As shown in Fig. 12(a), F-TENG output signal

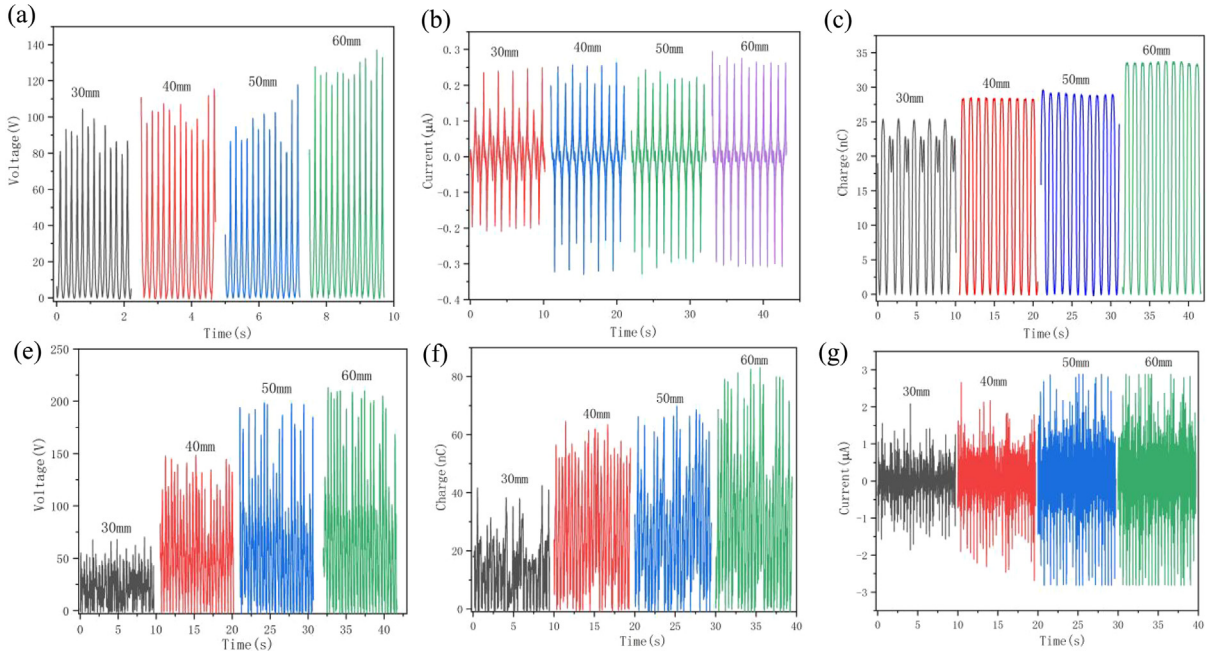

Fig. 11. The variation of ST-TENG output signal under different amplitude working conditions (a) F-TENG Open circuit voltage V_{OC}; (b) F-TENG short circuit current I_{ST}; (c) F-TENG transferred charge quantity Q; (d) CS-TENG Open circuit voltage V_{OC}; (e) CS-TENG short circuit current I_{ST}; (f) CS-TENG transferred charge quantity Q.

can be charged to the capacitor after rectifier rectification, and 3.3 μF and 10 μF capacitors can be charged to 9.26 V and 2.93 V respectively within 180 s (Fig. 12(b)). The CS-TENG output signal is rectified by a rectifier and charged to the capacitor (Fig. 12(c)). The capacitor can be charged to 11.16 V, 6.75 V, 2.26 V (Fig. 12(d)) for 90 s with 1 μF, 3.3 μF, and 33 μF capacitors, respectively. After CS-TENG and F-TENG are connected in series, LED lights are applied and capacitors are charged (Fig. 12(e)). The results show that the device can light at least 100 LED lights (Fig. 12(g)) and can charge 3.3 μF capacitors to 20.91 V within 150 s (Fig. 12(f)). This indicates that the device has certain output capacity, but because the current is low, the LED lamp cannot reach the maximum brightness, so it is not possible to capture all the lights that are on. In addition, the stability of the device is the key to ensure long-term power supply to the sensor. As shown in Fig. 12(h), 3000 cycles are made every other week, and the signal remains stable after three weeks. The following research can further optimize the device and apply it to underwater sensor power supply and indicator lights on the sea.

4. Conclusion

Traditional wave energy power generation technology often uses the principle of electromagnetic induction [3,4]. The difference is that based on the basic principle of triboelectric nanogenerator, this paper studies a swing ship type triboelectric nanogenerator for collecting low-frequency wave energy. Unlike traditional methods [5,6], the device not only has uncomplicated structure and low safeguard cost, but it is extremely conducive to the collection of low-frequency wave energy. Combined with experiments, the output electrical signal characteristics of ST-TENG under different internal structure conditions and external working conditions are studied in this paper. Specific experiments show that the device has certain output capacity and stability. The conclusions are as follows:

- Firstly, the structure of ST-TENG is analyzed, which showed obvious imparity with other TENGs using a single working mode for electricity generation [24–26], This paper combines the two working modes of free-standing layer and vertical contact separation to fully improve the space utilization efficiency. And the feasibility of using this device to efficiently collect wave energy is demonstrated by the operating principle analysis and electrostatic field simulation of ST-TENG.

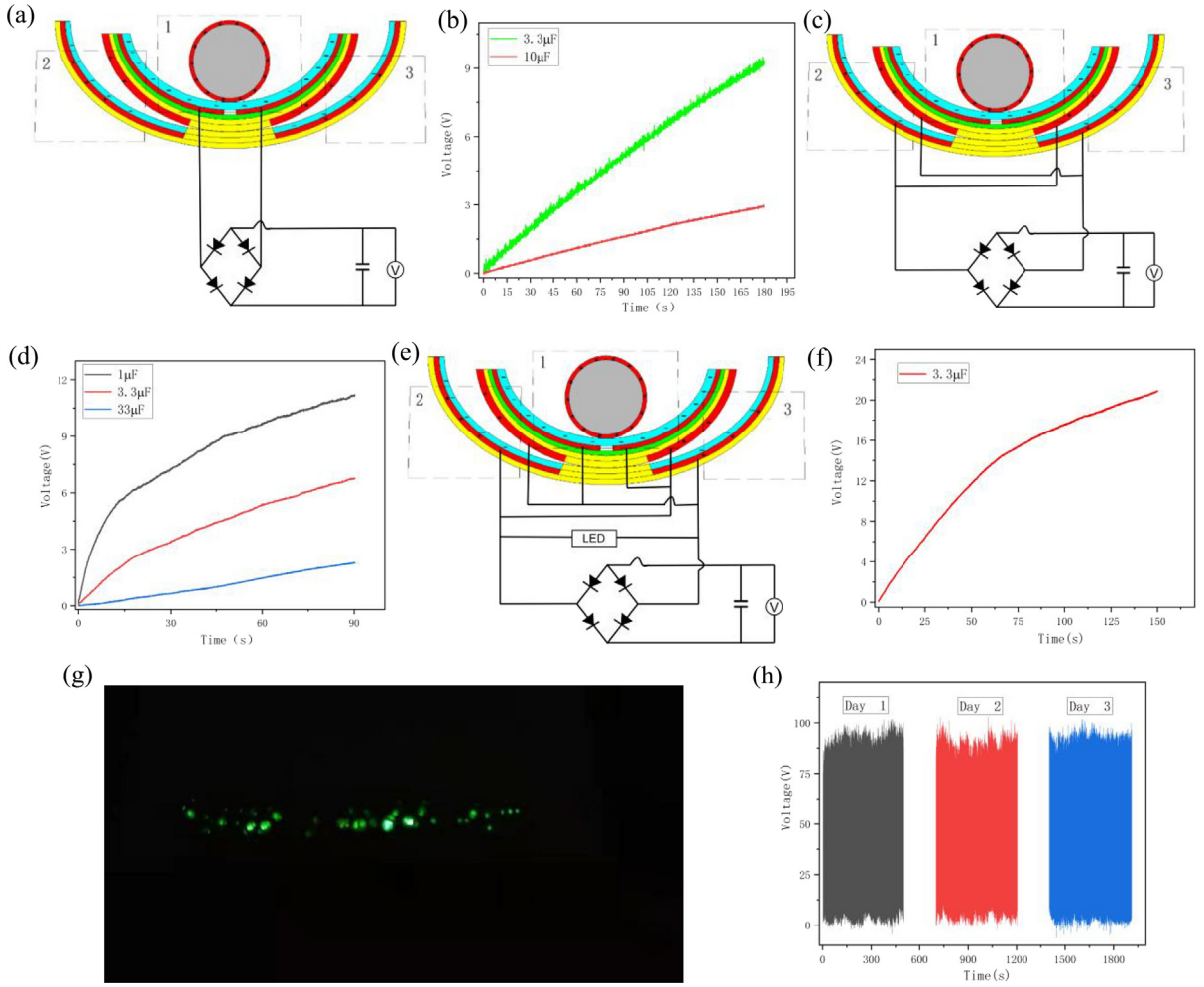

Fig. 12. (a) Schematic diagram of F-TENG connecting rectifier to charge capacitor; (b) Charging voltage of F-TENG to capacitors with different capacitors; (c) Schematic diagram of CS-TENG connecting rectifier to charge capacitor; (d) Charging voltage of CS-TENG to capacitors with different capacitors; (e) Schematic diagram of ST-TENG connecting rectifier to charge capacitor; (f) Charging voltage of ST-TENG to capacitors with different capacitors; (g) Lighting LED diagram; (h) ST-TENG stability test diagram.

- Experiments show that for the internal structure parameters, 0.3 mm PTFE as dielectric film has a strong output capacity, and the output performance is better than that of hollow roller when using a solid roller. With the addition of foam tape, the open circuit voltage and transfer charge of ST-TENG increase significantly. For external working conditions, 1.5 Hz is closest to the resonance frequency of the device, when the output is the highest, but the signal is unstable. As the amplitude increases from 30 mm to 60 mm, the open circuit voltage and transfer charge increase continuously, and the short-circuit current increases first and then remains unchanged.
- Charging and lighting experiments show that ST-TENG can charge the capacitor to a certain amount of power in a short time, and can power up at least 100 LED lights. In addition, the device has strong stability. Therefore, a new idea is provided for large-scale blue energy collection and practical application.

Declaration of competing interest

The authors declare that they have no known competing financial interests or personal relationships that could have appeared to influence the work reported in this paper.

Data availability

No data was used for the research described in the article.

Acknowledgments

The authors gratefully acknowledge the support provided for this research by Guangdong provincial special fund, China for promoting high quality economic development (Yuerong Office letter [2020]161, GDNRC [2021]56).

References

[1] Wang Zhong Lin. Catch wave power in floating nets. Nature 2017;542(7640):159–60.
[2] Clément Alain, Pat McCullen, António Falcao. Wave energy in Europe: Current status and perspectives. Renew Sustain Energy Rev 2002;6(5):405–31.
[3] Ahamed Raju, McKee Kristoffer, Howard Ian. Advancements of wave energy converters based on power take off (PTO) systems: A review. Ocean Eng 2020;204:107248.
[4] Zhao Tiancong, et al. Recent progress in blue energy harvesting for powering distributed sensors in ocean. Nano Energy 2021;88:106199.
[5] López Mario, et al. The wave energy converter CECO: current status and future perspectives. Multidiscip Digit Publ Inst Proc 2018;23:101423.
[6] Falcão António FO, Henriques Joao CC. Oscillating-water-column wave energy converters and air turbines: A review. Renew Energy 2016;85:1391–424.
[7] Wu Changsheng, et al. (2019)Triboelectric nanogenerator: a foundation of the energy for the new era. Adv Energy Mater 2019;9(1):1802906.
[8] Chun Sungwoo, et al. Self-powered pressure-and vibration-sensitive tactile sensors for learning technique-based neural finger skin. Nano Lett 2019;19(5):3305–12.
[9] Le Chau-Duy, et al. Liquid–solid contact electrification based on discontinuous-conduction triboelectric nanogenerator induced by radially symmetrical structure. Nano Energy 2021;80:105571.
[10] Liu Guoxu, et al. Self-powered electrostatic adsorption face mask based on a triboelectric nanogenerator. ACS Appl Mater Interfaces 2018;10(8):7126–33.
[11] Xu Wanghuai, et al. A droplet-based electricity generator with high instantaneous power density. Nature 2020;578(7795):392–6.
[12] He Tianyiyi, et al. Self-sustainable wearable textile nano-energy nano-system (NENS) for next-generation healthcare applications. Adv Sci 2019;6(24):1901437.
[13] Kim Inkyum, et al. Levitating oscillator-based triboelectric nanogenerator for harvesting from rotational motion and sensing seismic oscillation. Nano Energy 2020;72:104674.
[14] Xu Minyi, et al. A highly-sensitive wave sensor based on liquid–solid interfacing triboelectric nanogenerator for smart marine equipment. Nano Energy 2019;57:574–80.
[15] Garcia Cristobal, et al. Triboelectric nanogenerator as self-powered impact sensor. MATEC Web Conf 2018;148.
[16] Guo Huijuan, Li Tao, Cao Xiaotao, Wang ZhongLin. Self-sterilized flexible single-electrode triboelectric nanogenerator for energy harvesting and dynamic force sensing. ACS Nano 2017;11(1):856–64.
[17] Garcia Cristobal, et al. Self-powered acceleration sensor based on liquid metal triboelectric nanogenerator for vibration monitoring. ACS Nano 2017;11(7):7440–6.
[18] Lin Zong-Hong, et al. Water–solid surface contact electrification and its use for harvesting liquid-wave energy. Angew Chem Int Ed 2013;52(48):12545–9.
[19] Li Xiaoyi, et al. Networks of high performance triboelectric nanogenerators based on liquid–solid interface contact electrification for harvesting low-frequency blue energy. Adv Energy Mater 2018;8(21):1800705.
[20] Wen Xiaonan, et al. Harvesting broadband kinetic impact energy from mechanical triggering/vibration and water waves. ACS Nano 2014;8(7):7405–12.
[21] Wang Jiyu, et al. Rational structure optimized hybrid nanogenerator for highly efficient water wave energy harvesting. Adv Energy Mater 2019;9(8):1802892.
[22] Ahmed Abdelsalam, et al. Self-powered wireless sensor node enabled by a duck-shaped triboelectric nanogenerator for harvesting water wave energy. Adv Energy Mater 2017;7(7):1601705.
[23] Jiang Tao, et al. Robust swing-structured triboelectric nanogenerator for efficient blue energy harvesting. Adv Energy Mater 2020;10(23):2000064.
[24] Wang Xiaofeng, et al. Triboelectric nanogenerator based on fully enclosed rolling spherical structure for harvesting low-frequency water wave energy. Adv Energy Mater 2015;5(24):1501467.
[25] Cheng Ping, et al. Largely enhanced triboelectric nanogenerator for efficient harvesting of water wave energy by soft contacted structure. Nano Energy 2019;57:432–9.
[26] Xu Minyi, et al. High power density tower-like triboelectric nanogenerator for harvesting arbitrary directional water wave energy. ACS Nano 2019;13(2):1932–9.
[27] Liu Guanlin, et al. Power cables for triboelectric nanogenerator networks for large-scale blue energy harvesting. Nano Energy 2020;75:104975.